Journal of Power Sources 188 (2009) 627–634

Contents lists available at ScienceDirect

Journal of Power Sources

journal homepage: www.elsevier.com/locate/jpowsour

Characteristics of triphenylamine-based dyes with multiple acceptors in application of dye-sensitized solar cells

Chien-Hsin Yang[a,*], Han-Lung Chen[b], Yao-Yuan Chuang[c], Chun-Guey Wu[d], Chiao-Pei Chen[a], Shao-Hong Liao[a], Tzong-Liu Wang[a]

[a] Department of Chemical and Materials Engineering, National University of Kaohsiung, Kaohsiung 811, Taiwan
[b] Department of Chemical and Materials Engineering, Southern Taiwan University, Tainan 716, Taiwan
[c] Department of Applied Chemistry National University of Kaohsiung, Kaohsiung 811, Taiwan
[d] Department of Chemistry National Central University, Taoyuan 320, Taiwan

ARTICLE INFO

Article history:
Received 24 November 2008
Accepted 7 December 2008
Available online 13 December 2008

Keywords:
Dye-sensitized solar cells (DSSCs)
Triphenylamine-rhodanine dyes
Polyethylene oxide (PEO)-based electrolyte
Nanocrystalline TiO_2

ABSTRACT

We report the synthesis and photophysical/electrochemical properties of triphenylamine (TPA)-based multiple electron acceptor dyes (TPAR1, TPAR2, and TPAR3) as well as their applications in dye-sensitized solar cells (DSSCs). In these dyes, the TPA group and the rhodanine-3-acetic acid play the role of the basic electron donor unit and the electron acceptor, respectively. It was found that introduction of two rhodanine-3-acetic acid groups into the TPA unit (TPAR2) exhibited better photovoltaic performance due to the increase with a red shift and broadening of the absorption spectrum. The monolayer of these TPA-based dyes was adsorbed on the surface of nanocrystalline TiO_2 mesoporous electrode with the thickness of ~6 μm, polyethylene oxide (PEO) used as the matrix of gel electrolyte, and 4-nm thick Pt used as a counter-electrode. Photovoltaic device can be realized in a single quasi-solid-state DSSC. TPAR2-based gel DSSC had an open circuit voltage and short circuit current density of about 541 and 10.7 mA cm^{-2}, respectively, at 1-sun.

1. Introduction

Dye-sensitized solar cells (DSSCs) have received attention for transferring clean solar energy into electricity over the past decade [1,2]. The inorganic–organic hybrid DSSCs have been extensively investigated for the areas of designing more efficient dyes and electron mediators [2], fabricating better nanostructured films [3], and more deeply understanding the interfacial charge-transfer process [3–5]. In a DSSC device, light is absorbed by the dye anchored on the TiO_2 surface and then electrons from the excited dye inject into the conduction band of the TiO_2, generating electric current, while the ground state of the dye is regenerated by the electrolyte to give efficient charge-separation [6]. Thus, the dye in DSSCs is essential for efficient light harvesting and electron generation/transfer. The electrolyte, containing a redox couple I_3^-/I^- mediator, is injected into the slit between the anode and the catalytic Pt counter-electrode. A dye sensitizer needs efficient charge injection with photoexcitation [2]. To obtain high conversion efficiencies, it requires that the photogenerated electrons flow into the oxide film with minimal losses to interfacial recombination [3–5].

The connection between neighboring TiO_2 NPs plays an important role in achieving high light-to-electricity conversion efficiencies for DSSCs. Anatase TiO_2 has been proved the optimum choice of the semiconductor oxide for DSSCs. In sight of this, many efforts have been tried to improve the efficiency of electron transport by using TiO_2 nanostructures through the use of hydrothermal process [6,7]. Anatase TiO_2 nanoparticles from hydrothermal treatment on a titanate ($H_2Ti_2O_4(OH)_2$) which consists of lamellar sheets of edged-shared TiO_6 octahedra arranged in the zigzag construction [8,9]. The zigzag TiO_6 arrangement is the principal feature for the (1 0 1) face of anatase TiO_2, deriving from this titanate is expected to be phase pure and structure perfect resulting in a low electron trap density.

The typical sensitizer at the present time was N3 dye cis-$Ru(SCN)_2L_2$ (L = 2,2′-bipyridyl-4,4′-dicarboxylate) [2], which is grafted onto the semiconductor through anchoring groups, e.g. carboxylate that bind strongly to the oxide by the coordination of surface titanium ions. This ruthenium-complex sensitizer exhibits efficient charge injection after photoexcitation [2]. Owing to the use of rare metals and the difficulty of purification, many metal-free dyes have been investigated [10–15]. Among these dyes, the indoline dye [14,15] has demonstrated the promising high efficiency. In addition, this dye has the advantage that it can be produced at low cost, because it does not contain the expensive rare metal ruthenium and it is easy to synthesize. On the other hand, room

* Corresponding author. Tel.: +886 7 5919420.
E-mail address: yangch@nuk.edu.tw (C.-H. Yang).

0378-7753/$ – see front matter © 2008 Elsevier B.V. All rights reserved.
doi:10.1016/j.jpowsour.2008.12.026

temperature ionic liquid-based electrolytes have been developed to contribute in this field [16] and molten salts based on imidazolium iodides have showed excellent stability under prolonged light soaking [17,18].

In this study, we report on the synthesis and characterization of triphenylamine-based indoline dyes with multiple electron acceptors of rhodanine-3-acetic acid and their further application as sensitizers in DSSCs. Dyes were designed to create multiple channels of electron injection into TiO_2 electrode for enhancement in the efficiency of DSSCs. In the molecular design, TPAR1 is the basic model, in which the TPA unit was connected to one molecule of rhodanine-3-acetic acid. The second rhodanine-3-acetic acid was introduced to the adjacent phenyl ring of TPAR1, obtaining TPAR2 that has two electron acceptors. Similarly, the third rhodanine-3-acetic acid was attached to the third phenyl ring of TPAR2, yielding the structure of TPAR3. The introduction of multiple electron acceptors to the adjacent phenyl ring of TPA-based dyes would have a significant influence on the photovoltaic performance of the DSSCs.

2. Experimental details

2.1. Synthesis and characterization

The starting materials 4-formaltriphenylamine (FTPA), 4,4′-diformaltriphenylamine (DFTPA), 4,4′,4″-triformaltriphenylamine (TFTPA), were prepared by adopting literature procedure [19]. All other solvents and chemicals used in this work were analytical grade and were used without further purification. The synthetic pathway of the three dyes (TPAR1, TPAR2, and TPAR3) is shown in Scheme 1.

2.1.1. TPAR1

To 15 mL of glacial acetic acid were added 150 mg (0.55 mmol) of FTPA and 110 mg (0.57 mmol) of rhodanine-3-acetic acid and the solution was refluxed for 3 h in the presence of 100 mg of ammonium acetate. After cooling to room temperature, the mixture was poured into ice water. The precipitate was filtered and washed with distilled water. After drying under vacuum, the precipitate was purified by recrystallization from ethanol, obtaining red crystals of TPAR1 (190 mg, 75%). ^{1}H NMR (400 MHz, DMSO-d_6): δ (ppm): 4.70 (2H, s, $-CH_2COOH$), 6.9 (2H, d, J = 8.0 Hz, aromatic), 7.15–7.22 (6H, q, J = 19.2 Hz, aromatic), 7.40 (4H, t, J = 7.6 Hz, aromatic), 7.46 (2H, d, J = 8.4 Hz, aromatic), 7.73 (1H, s, –CH=).

2.1.2. TPAR2

A procedure similar to that for TPAR1 but with DFTPA (166 mg, 0.55 mmol) instead of FTPA and 220 mg (1.14 mmol) of rhodanine-3-acetic acid were used. ^{1}H NMR (400 MHz, DMSO-d_6): δ (ppm): 4.72 (4H, s, $-CH_2COOH$), 7.18 (4H, d, J = 8.8 Hz, aromatic), 7.24 (2H, d, J = 7.6 Hz, aromatic), 7.33 (1H, t, J = 7.6 Hz, aromatic), 7.47 (2H, t, J = 7.6 Hz, aromatic), 7.62 (4H, d, J = 8.8 Hz, aromatic), 7.84 (2H, s, –CH=).

2.1.3. TPAR3

A procedure similar to that for TPAR1 but with TFTPA (182 mg, 0.55 mmol) instead of FTPA and 330 mg (1.71 mmol) of rhodanine-3-acetic acid were used. ^{1}H NMR (400 MHz, DMSO-d_6): δ (ppm): 4.64 (6H, s, $-CH_2COOH$), 7.25 (6H, d, J = 8.8 Hz, aromatic), 7.67 (6H, d, J = 8.8 Hz, aromatic), 7.82 (3H, s, –CH=).

2.2. TiO_2 mesoporous electrode

The hydrothermal processed TiO_2 colloid was synthesized. In brief, 3 g TiO_2 nanoparticles (P25, Degussa AG, Germany, a mixture of ca. 30% rutile and 70% anatase) were dispersed in 100 mL 10N NaOH and heated to 130 °C in autoclave for 1 day. The precipitate was then re-dispersed in 100 mL 1N HNO_3. This suspension was subsequently subjected to autoclaving at 240 °C for 12 h to give the TiO_2 colloid. The TiO_2 specimens were baked at 450 °C in air for 30 min. The Raman spectra of TiO_2 nanoparticles, revealing that

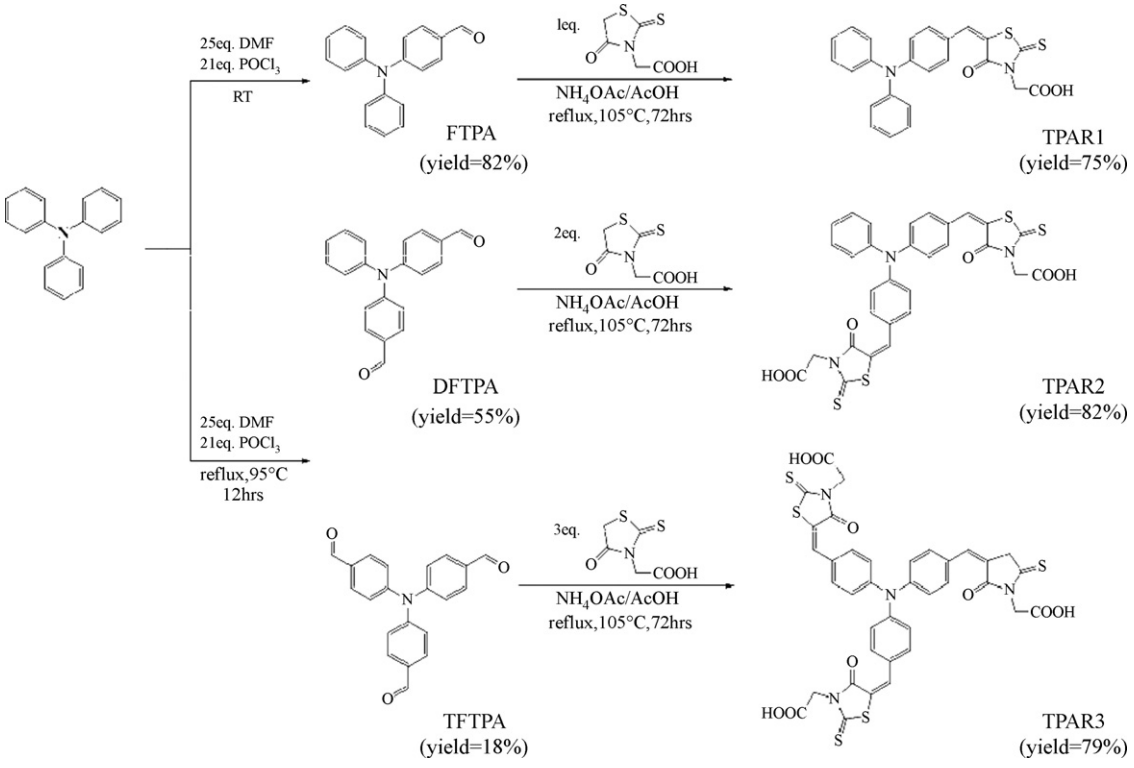

Scheme 1. Synthesis of TPAR dyes.

there existed a pure anatase phase corresponding to the wavenumbers of 150, 400, 517, and 638 cm^{-1}. X-ray diffraction (XRD) patterns of the titanate-derived TiO_2 also proved a pure anatase phase. The average crystal size was calculated, according to Scherrer's equation, to be approximately 20 nm. The solution of TiO_2 colloid was mixed with polyethylene glycol (PEG-2000) (Fluka) to form a viscous TiO_2 dispersion at a 0.15 of PEG/TiO_2 ratio, which was spin-coated onto a indium-tin oxide (ITO)-coated glass (Merck, sheet resistance of 10 $\Omega\,sq^{-1}$) to form a TiO_2 film of 0.25 cm^2. The thickness of TiO_2 film was controlled at ca. 6 μm. The film was dried in air at 120 °C for 30 min and calcined at 450 °C for 30 min.

2.3. Fabrication of DSSCs

The counter-electrode of platinum was coated onto an FTO glass (10 $\Omega\,sq^{-1}$, Hartford) by spin-coated processes. The dye-loaded anode and a Pt counter-electrode were sealed together with a sealing material, SX1170 (Solaronix), around the TiO_2 active area of 0.25 cm^2. The liquid-type electrolyte containing 0.6 M 1-propyl-2,3-dimethylimidazolium iodide (DMPII), 0.1 M lithium iodide, 0.05 M iodine, and 0.5 M 4-tert-butylpyridine (TBP) in 3-methoxypropionitrile (MPN) and the gel-type electrolyte extra-adding 10 wt.% polyethylene oxide (MW = 300,000) into the above liquid electrolyte were then introduced into the cells, respectively, forming liquid and gel-type DSSCs. The active area is 0.25 cm^2.

2.4. Measurements

^1H and ^{13}C NMR spectra were measured on a Bruker AV400 FT-NMR spectrometer (400 MHz). Infrared spectra were recorded on a Perkin–Elmer RXI FT-IR spectrometer. Absorption spectra were measured with a Perkin–Elmer Lambda 25 UV-visible spectrophotometer. The thickness of TiO_2 films was determined by an α-step instrument (Surfocorder TE 2400M, Tosaka Lab. Ltd.). Electrochemical experiments were performed using the electrochemical analyser (PGSTAT 30, AUTOLAB Electrochemical Instrument, The Netherlands). The current density–voltage (*J–V*) characteristics of the DSSCs were measured using Keithley-2400 digital source meter controlled by a computer at a scan rate of 10 mV s^{-1}. An Oriel 500 W xenon lamp served as the light source in connection with an AM 1.5 Globe filter (Oriel 81094) to remove ultraviolet and infrared radiation to give 100 mW cm^{-2} at the surface of the test cell. Calibration was performed by a USB 400 plug-and-play miniature fiber optic spectrometer (Ocean, USA) to give an AM 1.5 simulated sunlight. The active area of testing cell was 0.25 cm^2.

2.5. Computational methods

The Gaussian 03 package [20] was used for carrying out theoretical calculations. To model the electronic state of TPAR dyes on the TiO_2 surface, the dye's potassium salt was employed to simulate the dye bonded to TiO_2 surface in its carboxylate form. The B3LYP method with 6-31G(d) basis set was applied to optimize ground state geometries of TPAR1, TPAR2, and TPAR3. The minimum energy structures were confirmed by no imaginary frequency.

3. Results and discussion

3.1. Synthesis and characterization of TPAR dyes

The synthesis of TPAR dye proceeded following Scheme 1, and was confirmed by IR and NMR spectroscopy. Fig. 1 shows typical IR spectra for FTPA, DFTPA, TFTPA, TPAR1, TPAR2 and TPAR3, revealing characteristic IR absorption bands of the formaldehyde group at 1690 (C=O) and 2800 ((O=)C–H) cm^{-1}, respectively. These characteristic bands of the formaldehyde group on FTPA are absent through the reaction of Knoevenagel condensation with the methylene group on rhodanine-3-acetic acid forming a series of TPAR dyes. The characteristic bands of C=O and C–O–H on TPAR dyes present at 1710 and 1360 cm^{-1}, respectively. This indicates that the rhodanine-3-acetic acid has successfully attached onto TPA molecules forming a series of TPAR dyes. A typical set of ^1H and ^{13}C NMR spectra of TPAR in deuterated dimethyl sulfoxide (DMSO-d_6) are shown in Figs. 2 and 3, respectively. The assignment of hydrogen (see Section 2) and carbon atoms is shown in ^{13}C NMR (DMSO-d_6, δ, ppm) of Fig. 3 as follows. TPAR1 ^{13}C NMR (400 MHz, DMSO-d_6): δ (ppm): 45.15 (C^{12}), 117.35 (C^{10}), 119.47 ($C^{1,1'}$), 124.67 ($C^{3,3'}$), 125.55 (C^6), 126.38 (C^8), 130.18 ($C^{2,2'}$), 133.03 (C^7), 134.19 (C^9), 145.68 ($C^{4,4'}$), 150.35 (C^5), 166.62 (C^{11}), 167.54 (C^{13}), 193.04 (C^{14}). TPAR2 ^{13}C NMR (400 MHz, DMSO-d_6): δ (ppm): 45.27 ($C^{12,12'}$), 119.36 ($C^{10,10'}$), 123.17 (C^1), 126.49 (C^3), 127.17 ($C^{6,6'}$), 127.35 ($C^{8,8'}$), 130.53 (C^2), 132.94 ($C^{7,7'}$), 133.60 ($C^{9,9'}$), 145.11 (C^4), 148.73 ($C^{5,5'}$), 166.63 ($C^{11,11'}$), 167.49 ($C^{13,13'}$), 193.10 ($C^{14,14'}$). TPAR3 ^{13}C NMR (400 MHz, DMSO-d_6): δ (ppm): 46.02 ($C^{8,8',8''}$), 120.61 ($C^{6,6',6''}$), 124.98 ($C^{2,2',2''}$), 128.86 ($C^{4,4',4''}$), 129.84 ($C^{3,3',3''}$), 132.99 ($C^{5,5',5''}$), 147.80 ($C^{1,1',1''}$),

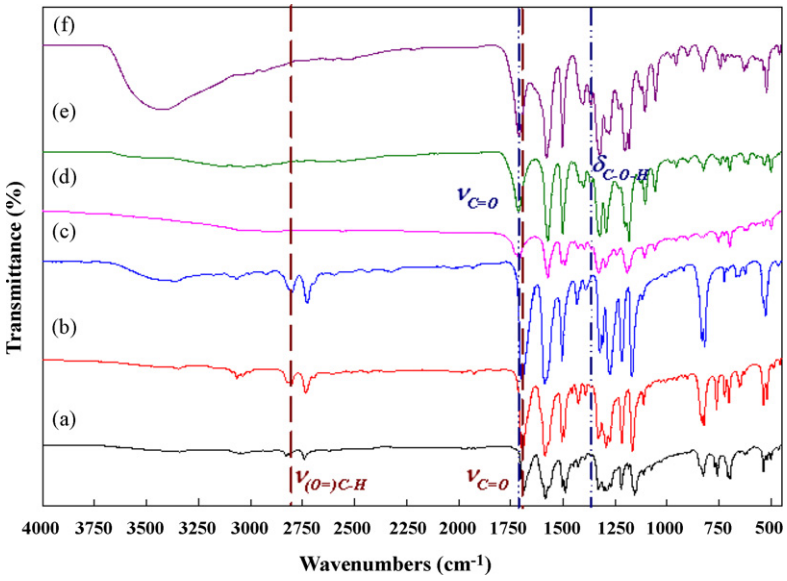

Fig. 1. FT-IR spectra of (a) FTPA, (b) DFTPA, (c) TFTPA, (d) TPAR1, (e) TPAR2, and (f) TPAR3.

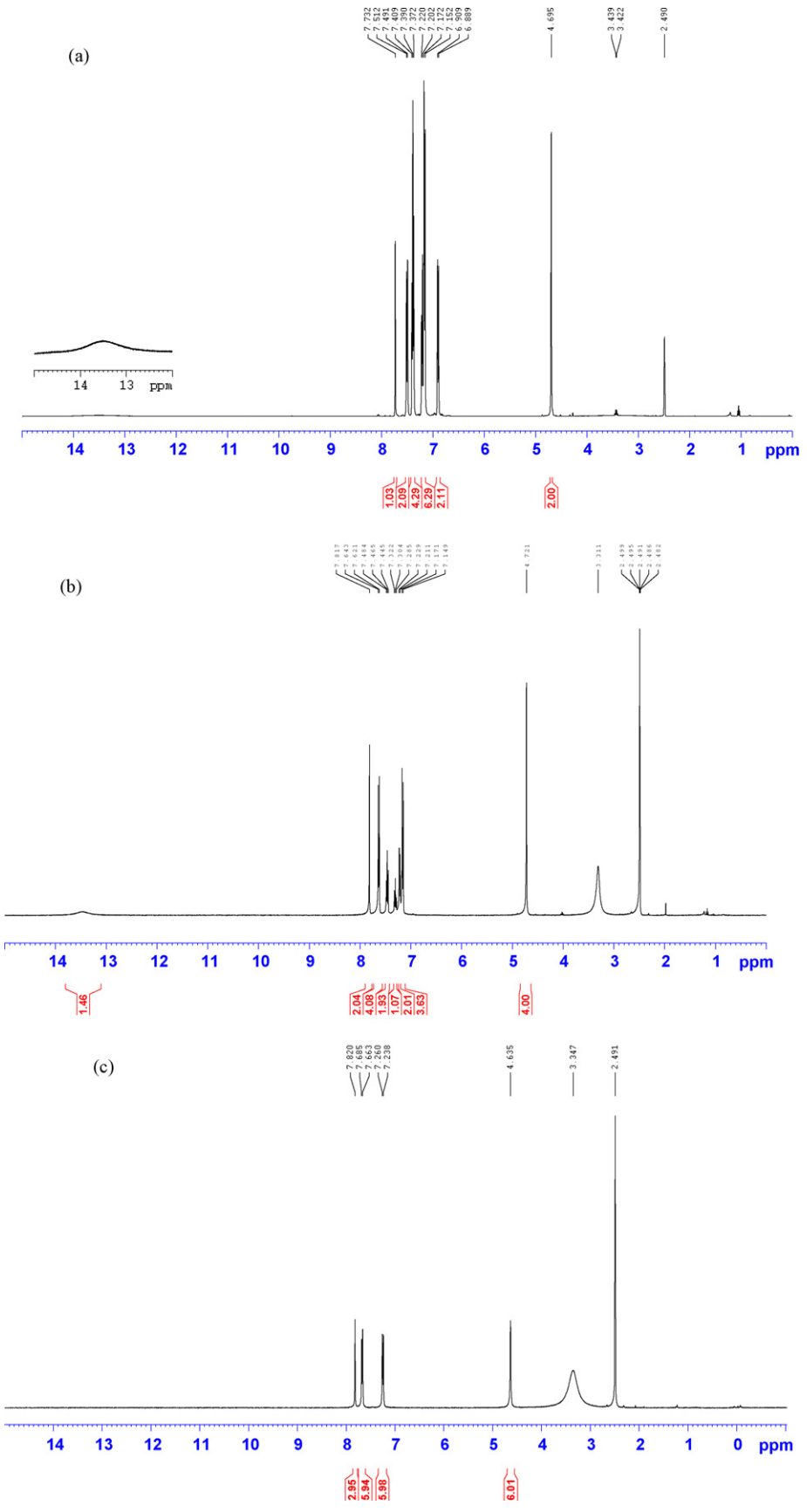

Fig. 2. ^{1}H NMR spectra of (a) TPAR1, (b) TPAR2, and (c) TPAR3 dyes in DMSO-d_6.

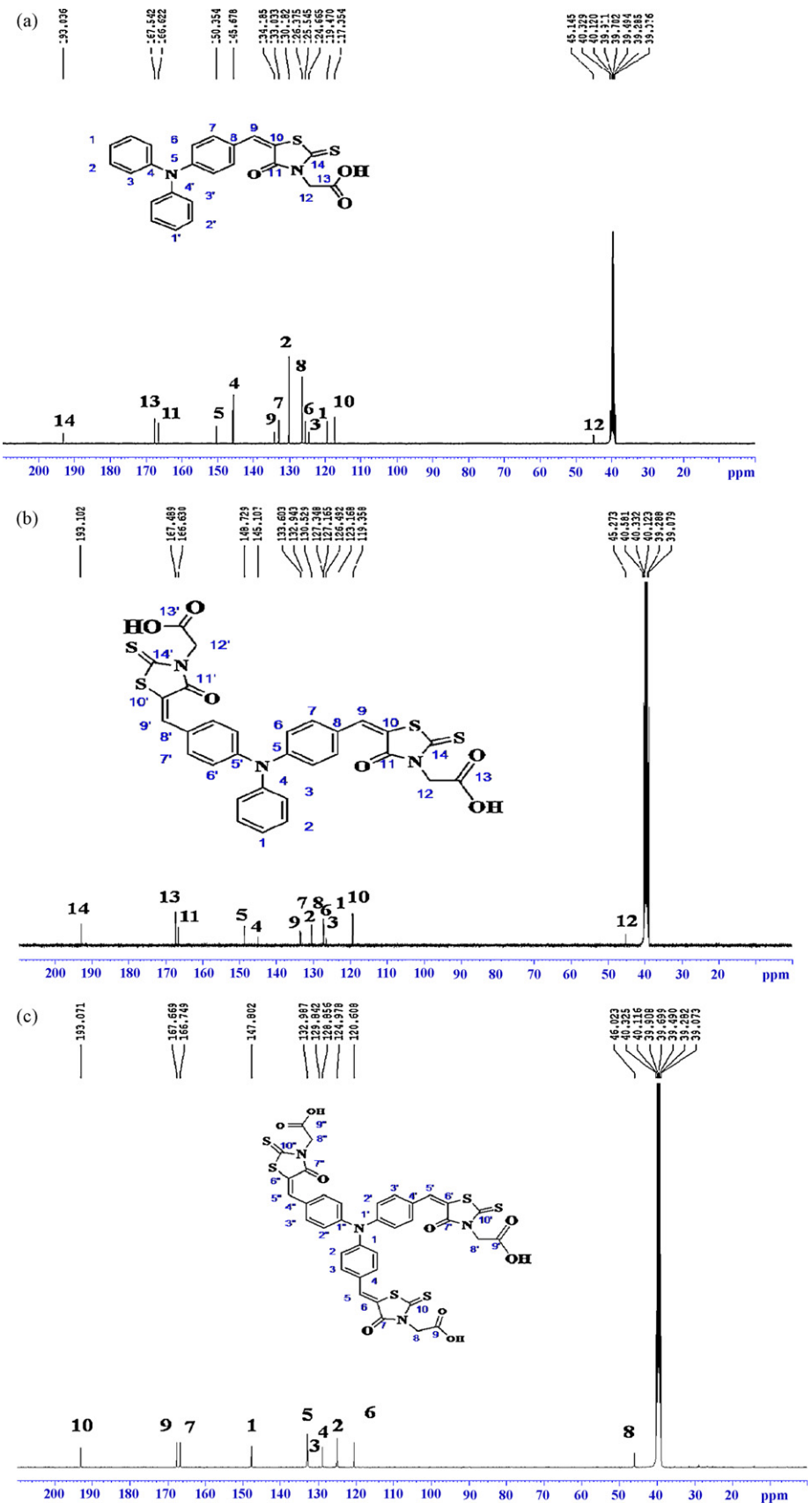

Fig. 3. ^{13}C NMR spectra of (a) TPAR1, (b) TPAR2, and (c) TPAR3 dyes in DMSO-d_6.

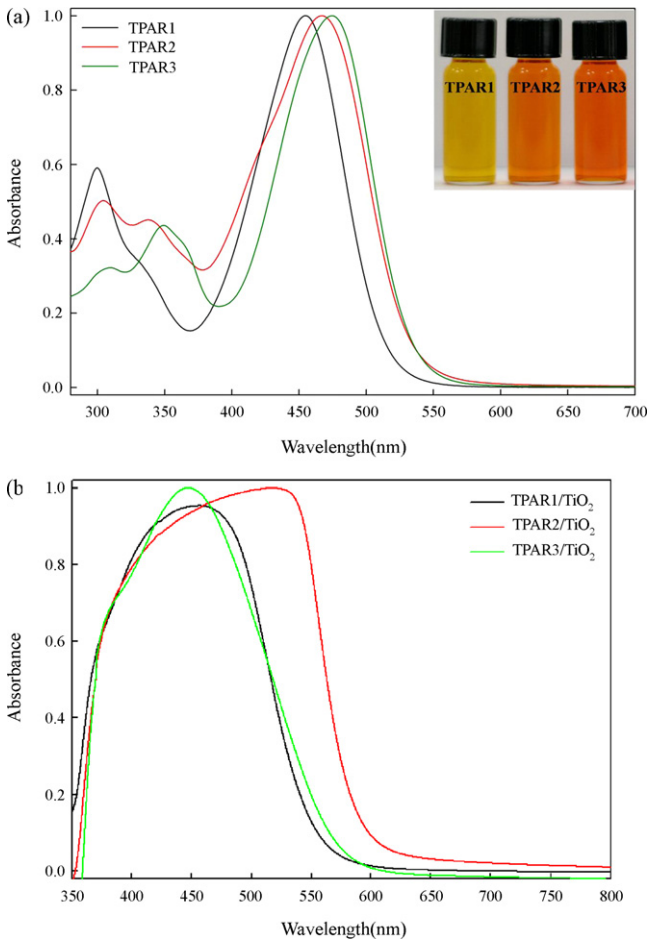

Fig. 4. (a) Absorption spectra of TPAR1, TPAR2, and TPAR3 dyes dissolved in ethanol and (b) absorption spectra of the as-synthesized dyes adsorbed on TiO_2 films, which were measured in the diffuse reflectance mode.

166.75 ($C^{7,7',7''}$), 167.67 ($C^{9,9',9''}$), 193.07 ($C^{10,10',10''}$). All the peaks have been assigned to the hydrogen and carbon atoms of the recurring unit. These spectra agree well with the proposed molecular structures of TPAR dyes.

3.2. Photophysical and electrochemical properties of dyes

Fig. 4(a) shows the absorption spectra of as-synthesized TPAR dyes in ethanol. The absorption spectrum of TPAR1 in ethanol displays two distinct absorption bands at around 300 and 455 nm, respectively. The weak absorption peaks at around 300 nm correspond to the $\Pi \rightarrow \Pi^*$ electron transition; strong absorption peaks at around 455 nm can be assigned to an intramolecular charge transfer between the TPA-based donor and the rhodanine-3-acetic acid [21], providing the efficient charge-separation at excited state. Note that the above two absorption bands are red-shifted with the increase of the groups of rhodanine-3-acetic acid in the dyes (TPAR2 and TPAR3). This is because the increase of electron acceptors in dye molecules is beneficial to intramolecular charge transfer. It is noteworthy that there exist intermediate state between the above two absorption bands in TPAR2 and TPAR3. This arises from the intervalence charge-transfer (IVCT) interactions within the triarylamine derivatives, the aminyl radical cations usually show absorption in the UV–vis region when the triarylamine derivatives were dissolved in acid-containing solvents [22]. The IVCT interactions increase with increasing the rhodanine-3-acetic acid because the entanglement of inter-molecules is more significant with the increase of the rhodanine-3-acetic acid. When the dyes adsorbed on the TiO_2 surface, the absorption spectra were generally red-shifted in relative to the dyes dissolved in ethanol, implying that most of dyes adsorbed on the TiO_2 surface with only partially J-type aggregates [21]. Note Fig. 4(b) that the absorption spectra of the adsorbed TPAR1 and TPAR2 dyes on the TiO_2 surface exhibit obvious red shifts in comparison with that of the two dyes in ethanol. This indicates that most of TPAR1 and TPAR2 dyes adsorbed on the TiO_2 surface with only partially J-type aggregates. TPAR3 dye is an exceptional case corresponding to a blue shift from 480 (in ethanol) to 447 nm (on TiO_2 surface) which almost overlaps with the spectra of TPAR1, because the three anchoring groups in TPAR3 dye-adsorbed on TiO_2 surface resulted in the scattering of electron acceptors within TPAR3 forming electron delocalization. The maximum absorption data are listed in Table 1, revealing that the extinction coefficient at maximum absorption increases with the increase of rhodanine ring.

Table 1
Maximum absorption data of the as-synthesized dyes.

Dye	ε (M^{-1} cm^{-1})[a]	UV λ_{max} (nm)[a]	UV λ_{max} (nm)[b]
TPAR1	35,264	455	460
TPAR2	44,827	467	519
TPAR3	54,656	480	447

[a] Absorption spectra of dyes measured in EtOH with the concentration of 5×10^{-5} M; ε is the extinction coefficient at maximum absorption.
[b] Absorption spectra of dyes adsorbed on TiO_2 photoelectrode.

Based on the Tauc relation [23], the energy gap (E_g) can be obtained by plotting $(\alpha h\nu)^2$ vs. $h\nu$ and extrapolating the linear portion of $(\alpha h\nu)^2$ to zero as shown in Fig. 5. The blue shift of TPAR3 dye can be evidenced by the higher energy band-gap as compared TPAR2 dye and closes to the value of TPAR1. The three anchoring groups in TPAR3 dye-adsorbed on TiO_2 surface resulted in the scattering of electron acceptors within TPAR3 forming electron delocalization, leading to a higher E_g.

We further calculate the molecular structures with bidentate carboxylate coordination to potassium as shown in Fig. 6. At the ground state (HOMO) for these dyes, electrons are homogeneously distributed in the electron donor groups. At the excited state (LUMO) with light illumination for TPAR1 and TPAR2 dyes, the intramolecular charge transfer occurs, resulting in the electron movement from the donor group to the acceptor groups (rhodanine rings). It is obvious that the acceptor groups on TPAR2 are more than that on TPAR1, indicating the more fluent movement of electrons with a lower E_g value in TPAR2, leading to the more efficient injection of electrons into TiO_2 photoelectrode for TPAR2. On the other hand, the intramolecular charge transfer only occurs two rhodanine rings in TPAR3 dye at the excited state, whereas the excited TPAR3

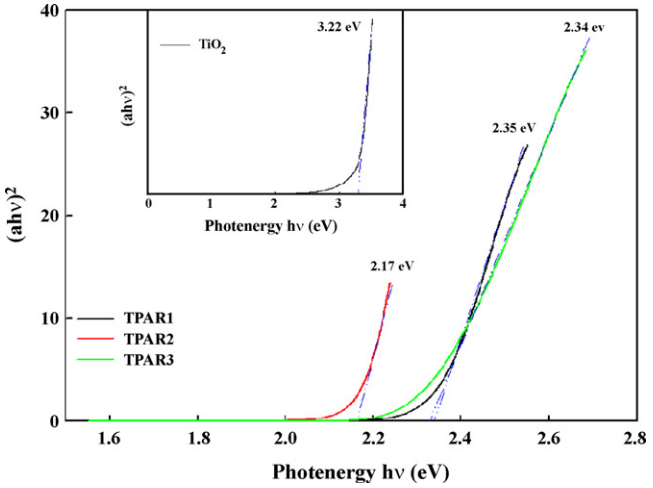

Fig. 5. Plot of $(\alpha h\nu)^2$ vs. $h\nu$.

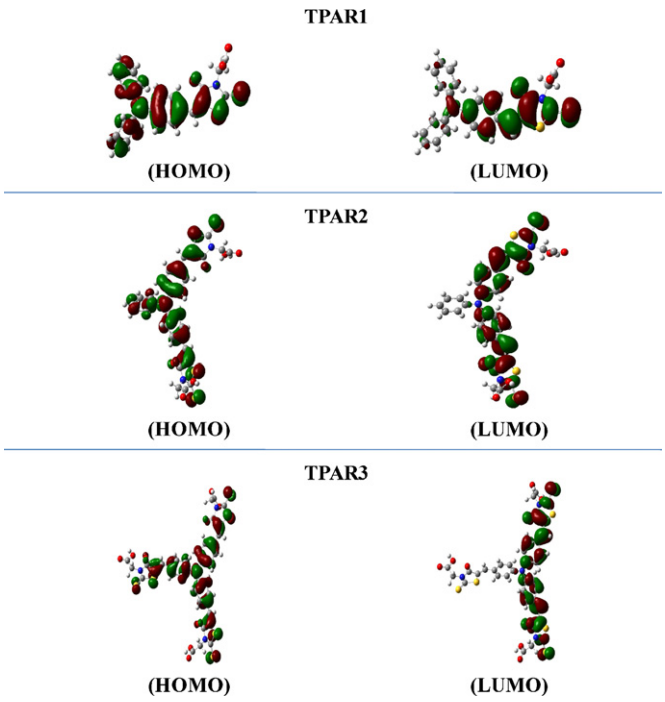

Fig. 6. The frontier orbitals of the potassium salt of TPAR dyes optimized at the B3LYP/6-31+G(d) level.

molecule remains one un-occupied-electron rhodanine ring. This un-occupied ring possesses attraction for the electrons on other two occupied-electron rings, resulting in the delocalization of the excited electrons in TPAR3. This electron delocalization leads to a lower injection efficiency of electrons into TiO_2 photoelectrode. Thus, the E_g value of TPAR3 becomes close to that of TPAR1.

Cyclic voltammogram (CV) is a preliminary characterization technique to determine the redox properties of organic and polymeric materials. The highest occupied molecular orbital (HOMO) and lowest un-occupied molecular orbital (LUMO) energy levels of the TPAR dyes could be determined from the $E_{1/2}$ (Fig. 7) and the onset absorption wavelength (E_g, energy band-gap) (Fig. 5) [24]. Fig. 7 shows the CVs of TPAR dyes adsorbed on TiO_2 films in acetonitrile/AcOH (7/1, v/v) solution containing 0.1 M tetrabutylammonium tetrafluoroborate ($TBABF_4$). The oxidation onset potential for TPAR dye has been determined as 0.38 V vs. Ag/Ag^+. The external ferrocene/ferrocenium (Fc/Fc^+) redox standard $E_{1/2}$ is

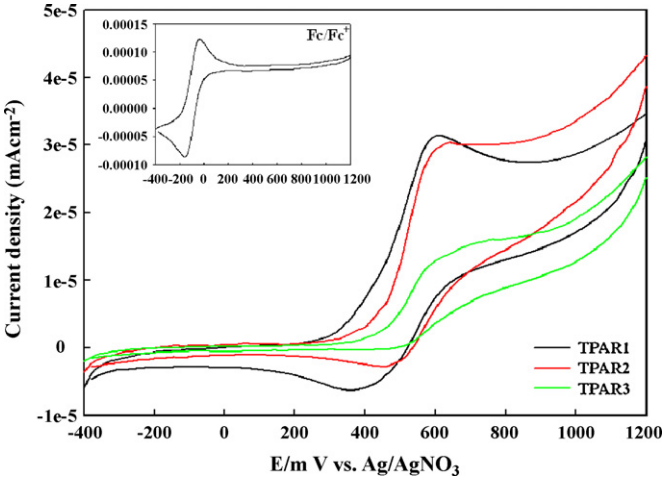

Fig. 7. CVs of TPAR1, TPAR2, and TPAR3 films on an ITO substrate in CH_3CN/AcOH containing 0.1 M tetrabutylammonium perchlorate at a scan rate of 10 mV s^{-1}. The inset is the CV of ferrocene.

Table 2
Optical and electrochemical properties of TPAR dyes.

Dye	Reduction (V vs. Ag/Ag^+)	Oxidation (V vs. Ag/Ag^+)	HOMO (eV)	E_g (eV)	LUMO (eV)
TPAR1	0.39	0.60	5.36	2.34	3.02
TPAR2	0.44	0.60	5.41	2.17	3.24
TPAR3	0.45	0.60	5.42	2.32	3.01

−0.1 V vs. Ag/Ag^+. Assuming that the HOMO energy for the Fc/Fc^+ standard is 4.80 eV with respect to the zero vacuum level, the HOMO energy for the TPAR1 dye has been evaluated to be 5.08 eV. The LUMO level can be determined from their HOMO and energy band-gap (E_g), and the results are listed in Table 2.

3.3. Solar cell performance

Light irradiation from a 500 W xenon lamp was focused through a monochromator onto the testing photovoltaic cell. The incident photon-to-current conversion efficiency (IPCE) of a DSSC was estimated between 400 and 800 nm according to the following equation [5]:

$$\mathrm{IPCE}(\lambda) = \frac{1240 J_{sc}(\mathrm{mA\,cm^{-2}})}{\lambda(\mathrm{nm})\psi(\mathrm{mW\,cm^{-2}})} \quad (1)$$

where λ is the wavelength and ψ is the power of the incident radiation per unit area. Light intensity was measured using a USB 400 fiber optic spectrometer. Fig. 8 shows the IPCE of the liquid electrolyte-type DSSCs as a function of the wavelength. It is obvious that the photocurrent response of TPAR2-sensitized DSSC has a higher value exceeding 75% in the range of 470–500 nm as compared TPAR1 and TPAR3 dyes. The maximum IPCE value of 80% occurs at 475 nm. The decrease of the IPCE above 600 nm in the long-wavelength region is attributed to the decrease of light harvesting for these dyes. The lower photocurrent response of TPAR1 and TPAR3-sensitized devices is ascribed to the blue shift dye with higher energy band-gap as compared TPAR2 dye. A similar data acquisition system was used to obtain the overall efficiency (η) of a DSSC device. The value of η is calculated from the short current density (J_{sc}), the open voltage (V_{oc}), the fill factor of the cell (FF), and the intensity of the incident light (P_{in}) as follows [5]:

$$\eta = \frac{J_{sc}V_{oc}(\mathrm{FF})}{P_{in}} \quad (2)$$

The *J–V* curves of the liquid electrolyte-type DSSCs are shown in Fig. 9, revealing that the curve of TPAR2-based DSSC is also higher

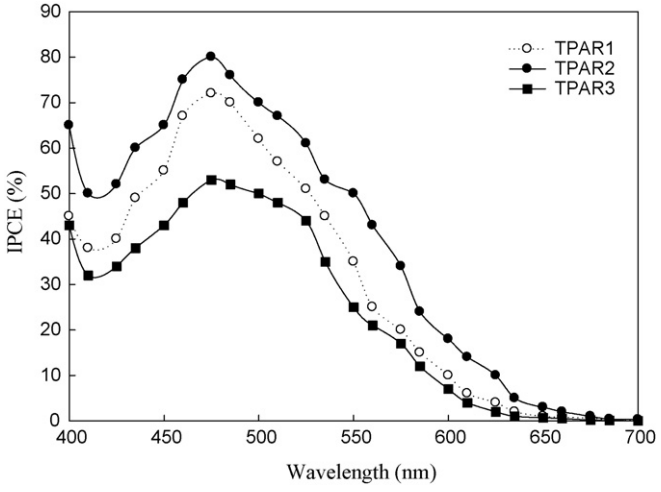

Fig. 8. IPCE spectra for the liquid-type DSSCs based on different dyes under AM 1.5 irradiation (100 mW cm^{-2}).

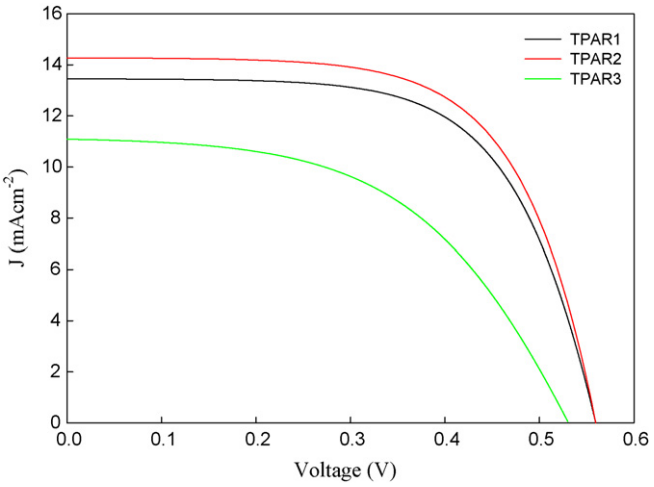

Fig. 9. Photocurrent–voltage (*J–V*) characteristics for the liquid-type DSSCs based on different dyes under AM 1.5 irradiation (100 mW cm^{-2}).

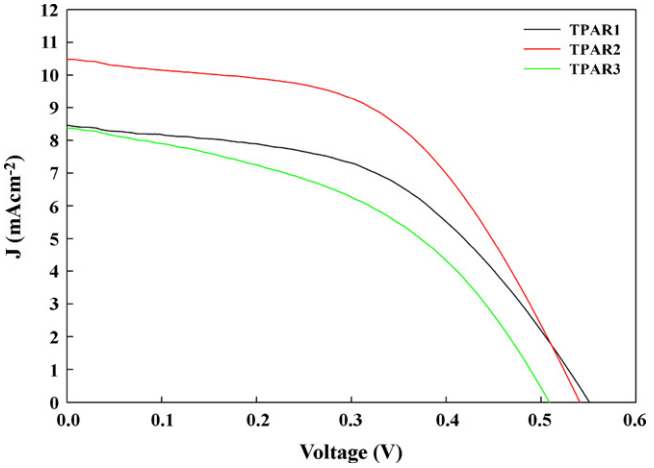

Fig. 10. Photocurrent–voltage (*J–V*) characteristics for the gel-type DSSCs based on different dyes under AM 1.5 irradiation (100 mW cm^{-2}).

than that of TPAR1 and TPAR3-based DSSCs. Fig. 10 shows the *J–V* curves of the gel electrolyte-type DSSCs. Also note that the curve of TPAR2-based DSSC is higher than that of TPAR1 and TPAR3-based DSSCs. These results are consistent with that of IPCE measurements. The photovoltaic data were summarized in Table 3. An examination of Table 3 reveals that the respective overall efficiencies of TPAR1 and TPAR3-sensitized DSSCs are lower about 10 and 37% than those of TPAR2-sensitized DSSCs in liquid electrolyte system. The explanation is similar to that of IPCE. It is noteworthy that the photovoltaic data of gel-type DSSCs are significantly lower ca. 33–44% than those of liquid-type DSSCs for the three dyes. This is because the in-series resistance in DSSCs would be increased with adding PEO gel polymer into the liquid electrolyte, and the transfer rate of redox species (I_3^-/I^-) in gel-type electrolyte is slowed down in relative to that in liquid-type electrolyte. These results reflect lower values of J_{sc}, V_{oc}, and FF. The above results are well agreed with those of E_g, UV–vis, and frontier orbital analyses.

Table 3
Photovoltaic performance of DSSCs sensitized with as-synthesized TPAR dyes.

Dye	Electrolyte-type	J_{sc} (mA cm^{-2})	V_{oc} (mV)	FF	η (%)
TPAR1	Liquid	13.2	562	0.58	4.28
	Gel	8.56	551	0.50	2.37
TPAR2	Liquid	14.2	560	0.60	4.77
	Gel	10.7	541	0.52	3.02
TPAR3	Liquid	11.0	530	0.51	2.97
	Gel	8.43	510	0.46	1.98

4. Conclusions

We demonstrated triphenylamine-based metal-free organic TPAR dyes that can be employed as light sensitizers in DSSCs. These dyes were designed to different content of rhodanine-3-acetic acid bearing on their molecular structures and exhibited photovoltaic and electrochromic performance. TPAR2 dye had two anchoring groups (rhodanine-3-acetic acid) possessing the optimal photovoltaic performance. Three anchoring groups on the dye molecules (TPAR3) decreased IPCE. It is noted that TPAR2-sensitized DSSCs showed higher η about 32% in relative to TPAR1 and TPAR3-sensitized DSSCs under AM 1.5 irradiation (100 mW cm^{-2}). It is also found that the efficiency of liquid-type DSSCs is higher about 47% than that of gel-type DSSCs.

Acknowledgements

Financial support from the Education Ministry (No. 0960190683Q) and National Science Council in Taiwan (NSC 96-2622-E-390-006-CC3, NSC-96-2221-E-390-020, and NSC-97-2221-E-390-013) are gratefully acknowledged.

References

[1] B. O'Regan, M. Gratzel, Nature 353 (1991) 737.
[2] M.K. Nazeeruddin, A. Kay, I. Rodicio, R. Humphry-Baker, E. Muller, P. Liska, N. Vlachopoulos, M. Gratzel, J. Am. Chem. Soc. 115 (1993) 6382.
[3] S.Y. Huang, G. Schlichthorl, A.J. Nozik, M. Gratzel, A.J. Frank, J. Phys. Chem. B 101 (1997) 2576.
[4] T. Oekermann, D. Zhang, T. Yoshida, H. Minoura, J. Phys. Chem. B 108 (2004) 2227.
[5] G. Boschloo, A. Hagfeldt, J. Phys. Chem. B 109 (2005) 12093.
[6] M.D. Wei, Y. Konishi, H.S. Zhou, H. Sugihara, H. Arakawa, J. Electrochem. Soc. 153 (2006) A1232.
[7] J.T. Jiu, S. Isoda, F.M. Wang, M. Adachi, J. Phys. Chem. B 110 (2006) 2087.
[8] C.C. Tsai, H.S. Teng, Chem. Mater. 18 (2006) 367.
[9] J. Yang, Z. Jin, X. Wang, W. Li, J. Zhang, S. Zhang, X. Guo, Z. Zhang, Dalton Trans. (2003) 3898.
[10] S. Ferrere, A. Zaben, B.A. Gregg, J. Phys. Chem. B 101 (1997) 4490.
[11] K. Hara, K. Sayama, Y. Ohga, A. Shinpo, S. Suga, H. Arakawa, Chem. Commun. (2001) 569.
[12] H. Tokuhisa, P.T. Hammond, Adv. Funct. Mater. 13 (2003) 831.
[13] K. Sayama, K. Tsukagoshi, T. Mori, K. Hara, Y. Ohga, A. Shinpo, Y. Abe, S. Suga, H. Arakawa, Sol. Energy Mater. Sol. Cells 80 (2003) 47.
[14] L. Schmidt-Mende, U. Bach, R. Humphry-Baker, T. Horiuchi, H. Miura, S. Ito, S. Uchida, M. Gratzel, Adv. Mater. 17 (2005) 813.
[15] T. Horiuchi, H. Miura, K. Sumioka, S. Uchida, J. Am. Chem. Soc. 126 (2004) 12218.
[16] W. Kubo, T. Kitamura, K. Hanabusa, Y. Wada, S. Yanagida, Chem. Commun. (2002) 374.
[17] P. Wang, S.M. Zakeeruddin, P. Comte, I. Exner, M. Gratzel, J. Am. Chem. Soc. 125 (2003) 1166.
[18] H.J. Byker, Gentex Corp., U.S. Patent no. 4,902,108 1990.
[19] M. Behl, E. Hattemer, M. Brehmer, R. Zentel, Macromol. Chem. Phys. 203 (2002) 503.
[20] M.J. Frisch, G.W. Trucks, H.B. Schlegel, G.E. Scuseria, M.A. Robb, J.R. Cheeseman Jr., J.A. Montgomery, T. Vreven, K.N. Kudin, J.C. Burant, J.M. Millam, S.S. Iyengar, J. Tomasi, V. Barone, B. Mennucci, M. Cossi, G. Scalmani, N. Rega, G.A. Petersson, H. Nakatsuji, M. Hada, M. Ehara, K. Toyota, R. Fukuda, J. Hasegawa, M. Ishida, T. Nakajima, Y. Honda, O. Kitao, H. Nakai, M. Klene, X. Li, J.E. Knox, H.P. Hratchian, J.B. Cross, V. Bakken, C. Adamo, J. Jaramillo, R. Gomperts, R.E. Stratmann, O. Yazyev, A.J. Austin, R. Cammi, C. Pomelli, J.W. Ochterski, P.Y. Ayala, K. Morokuma, G.A. Voth, P. Salvador, J.J. Dannenberg, V.G. Zakrzewski, S. Dapprich, A.D. Daniels, M.C. Strain, O. Farkas, D.K. Malick, A.D. Rabuck, K. Raghavachari, J.B. Foresman, J.V. Ortiz, Q. Cui, A.G. Baboul, S. Clifford, J. Cioslowski, B.B. Stefanov, G. Liu, A. Liashenko, P. Piskorz, I. Komaromi, R.L. Martin, D.J. Fox, T. Keith, M.A. Al-Laham, C.Y. Peng, A. Nanayakkara, M. Challacombe, P.M.W. Gill, B. Johnson, W. Chen, M.W. Wong, C. Gonzalez, J.A. Pople, Gaussian 03, Revision D. 01, Gaussian, Inc., Wallingford, CT, 2004.
[21] M. Liang, W. Xu, F. Cai, P. Chen, B. Peng, J. Chen, Z. Li, J. Phys. Chem. C111 (2007) 4465.
[22] C.H. Yang, L.R. Huang, F.J. Liu, T.L. Wang, W.C. Lin, M. Sato, C.H. Chen, C.C. Chang, J. Electroanal. Chem. 617 (2008) 101.
[23] C.H. Yang, T.C. Yang, J. Phys. Chem. Solid 69 (2008) 769.
[24] C.H. Yang, L.R. Huang, S.L. Chung, T.C. Wen, M.S. Tsai, J. Phys. Chem. C 111 (2007) 9227.